ACS APPLIED MATERIALS & INTERFACES

Article

Real-time Study of the Interaction between G-rich DNA Oligonucleotides and Lead Ion on DNA Tetrahedron-functionalized Sensing Platform by Dual Polarization Interferometry

Shuang Wang, Shasha Lu, Jiahui Zhao, Jianshe Huang, and Xiurong Yang

ACS Appl. Mater. Interfaces, **Just Accepted Manuscript** • DOI: 10.1021/acsami.7b13477 • Publication Date (Web): 03 Nov 2017

ACS Publications

ACS Applied Materials & Interfaces is published by the American Chemical Society.
1155 Sixteenth Street N.W., Washington, DC 20036

Real-time Study of the Interaction between G-rich DNA Oligonucleotides and Lead Ion on DNA Tetrahedron-functionalized Sensing Platform by Dual Polarization Interferometry

Shuang Wang,[†,‡] Shasha Lu,[†,‡] Jiahui Zhao,[†,§] Jianshe Huang,[†] and Xiurong Yang[,†]*

† State Key Laboratory of Electroanalytical Chemistry, Changchun Institute of Applied Chemistry, Changchun, Jilin 130022, China

‡ University of Science and Technology of China, Anhui 230026, China

§ University of Chinese Academy of Sciences, Beijing 100039, China

KEYWORDS: G-quadruplex, biomolecules interaction, dual polarization interferometry, DNA tetrahedron, detection of lead ions

ABSTRACT: G-quadruplex plays roles in numerous physiological and pathological processes of organisms. Due to the unique properties of G-quadruplex, (e.g. forming G4/hemin complexes with catalytic activity and electron acceptability, binding with metal ions, proteins, fluorescent ligands and so on) it has been widely applied in biosensing. But the formation process of G-

quadruplex is not yet to be fully understood. Here, a DNA tetrahedron platform with higher reproducibility, regenerative ability, and time-saving building process was coupled with dual polarization interferometry (DPI) technique for the real-time and label-free investigating the specific interaction process of guanine-rich singled-stranded DNA (G-rich ssDNA) and Pb^{2+}. The oriented immobilization of probes greatly decreased the spatial hindrance effect and improved the accessibility of the probes to the Pb^{2+} ions. Through the real-time monitoring the whole formation process of the G-quadruplex, we speculated the probes on the tetrahedron platform initially stood on the sensing surface with a random coil conformation, then the G-rich ssDNA preliminarily formed unstable G-quartets by H-bonding and cation binding, subsequently formed completely folded and stable quadruplex structure through relatively slow strand rearrangements. Based on these researches, we also developed a novel sensing platform for the specific and sensitive determination of Pb^{2+} and its chelating agent EDTA. This study not only provides a proof-of-concept for conformational dynamics of G-quadruplex-related drugs and pathogenes, but also enriches the biosensor tools by combining nanomaterial with interfaces technique.

INTRODUCTION

Growing studies demonstrate the implication of G-quadruplex formed by G-rich nucleotide sequence in major human diseases e.g. cancer, neurodegenerative diseases. Since the presence of G-quadruplex can suppress telomerase activity, the ligands that can stabilize G-quadruplex have great significance for cancer therapeutics.[1-5] In addition, recent studies have found that G-quadruplex has close relationship to neurodegenerative diseases.[6-8] For instance, a study identified quardruplex-containing tiRNAs as leading compounds for the designing of a series of

neuroprotective drugs due to its cytoprotective and prosurvival functions.[9] And G-quadruplex can be recognized by scavenger receptor A that improve the ability to enter the cell in the brain, which provide a new therapy direction for brain diseases.[10] Therefore, it is greatly significance to study the formation process of G-quadruplex for the identification of pathogenes and screen of drugs in the preliminary stage.

Numerous methods have been developed to study the formation process of G-quadruplex. The spectroscopic methods (eg. CD[11], UV[12], FRET[13,14], smFRET[15,16]) could supply sensitive quadruplex structural information, but the thermodynamic parameters were obtained only by fitting the specific models. The calorimetry (differential scanning calorimetry[17,18], isothermal titration calorimetry[19], pressure-perturbation calorimetry[20]) could be employed to directly monitor enthalpy changes and the parameters could be acquired in a model-free way, but it needs high concentrations and amounts of sample. Besides, other methods such as AFM[21], stopped-flow mixing technique[22,23], molecular dynamics simulations[24], and magnetic tweezers[25, 26]have also been skillfully employed in the study on the dynamic formation process of G-quadruplex. However, most of these methods were intended to indirectly confirm the structural transformation by spectra, energies and forces changes, and the structural information obtained was often single. Therefore, a method that could directly and real-time record the multiple well-understood structure information (such as thickness, density, mass) will supply a good supplements for above employed methods, and are beneficial for the researchers to better understand the formation process of G-quadruplex.

Dual polarization interferometry (DPI) tactfully utilizes solid-liquid interface technique to fulfill label-free and quantitative sensor response function, and simultaneously completes real-time and time-efficient demonstration of multiple kinetic conformation information. DPI

demonstrates higher sensitivity (below 50 Da) than surface plasmon resonance (SPR) as an optical interferometry,[27-29] and the mass sensitivity (0.1 pg/mm^2) of DPI is higher than the well-established electrochemical quartz crystal microbalance (EQCM) (50 pg/mm^2) as mass inspection technique.[30,31] Furthermore, compared with nuclear magnetic resonance (NMR)[32], X-ray crystallography[33], and neutron reflectivity (NR)[34], DPI can perfect the real-time function as a structural measurement technique. Therefore, DPI has been extensively applied in different fields, for instance, surface science, materials science, crystallography, and biomedicine.

As a surface-based biomolecule detection technique, it is inevitable that the accessibility of probes to the target molecules on a solid-liquid interface is reduced when compared with probe-target recognition in a homogenous solution.[35,36] In order to confront this challenge, the researchers constructed different sensing platforms. For instance, our group established anti-fouling aptasensor platform[37] and layer-by-layer assembly platform[38,39] for avoiding nonspecific adsorption. Au-S bond[35] and biotin-NeutrAvidin interaction[40] were also used for the oriented immobilization of ssDNA probes. Although the great progress had been made in the probe immobilization method, the accessibility problem remains a great challenge. Due to the mechanical rigidity, structural stability, high controllability and precision of DNA nanostructures,[41-44] recently, a three-dimensional (3D) DNA tetrahedron nanostructure has been introduced to effectively improved recognition of bioprobes[45-51] (e.g., DNA, antibodies, cancer cells, small molecules and so on). The probes could be orderly distributed at defined nanoscale distances on the interface, thereby reducing the interference from surroundings, enhancing the accessibility of probe. Combined the highly ordered DNA tetrahedron nanostructure with the DPI technique, a novel method was developed for the study of the dynamic conformation transition process of G-rich ssDNA induced by Pb^{2+}. Furthermore, label-free and sensitive

determination of Pb^{2+} and EDTA were completed by virtue of the DNA tetrahedron platform.

EXPERIMENTAL SECTION

Chemicals and apparatus. Poly (ethyleneimine) solution (PEI, 50% in H_2O, MW.750000) and (3-aminopropyl) trimethoxysilane (APTES) were obtained from Sigma-Aldrich (St Louis, MO). Magnesium chloride hexahydrate ($MgCl_2 \cdot 6H_2O$), zinc chloride ($ZnCl_2$), manganese (II) chloride ($MnCl_2$), and lead (II) acetate trihydrate [$Pb(Ac)_2 \cdot 3H_2O$] were obtained from Aladdin Chemistry Co. Ltd (St Louis, MO). Potassium chloride (KCl), cesium chloride (CsCl), calcium chloride ($CaCl_2$), sodium carbonate (Na_2CO_3), sodium acetate (NaAc), sodium formate (HCOONa) and sodium nitrate ($NaNO_3$) were provided from Beijing Chemical Reagent Co. (Beijing, China). Tris (hydroxymethyl) aminomethane (Tris, Ultrapure grade) was purchased from Amresco (Shanghai, China). Bis (sulfosuccinimidyl) suberate sodium salt (BS^3) was obtained from Thermo Fisher Scientific. All ssDNA oligonucleotides (Table S1) were synthesized by Sangon Biotechnology Co. Ltd. (Shanghai, China). All injected samples were prepared with 25 mM HEPES buffer solution. The ultrapure water of 18.25 MΩ•cm from Milli-Q water system were used in experiments.

CD spectra were measured on a Jasco J-820 circular dichroism spectra polarimeter (Tokyo, Japan). UV-Vis absorption spectra were performed by a CARY 500 UV-Vis-NIR Varian spectrophotometer. The CD and UV-Vis differential spectrometry were obtained by subtracting CD and UV-Vis spectra of tetrahedron probe with Pb^{2+} from that without Pb^{2+}. AFM images were collected on a Digital Instruments Nanoscope V (DI, Santa Barbara, CA) in tapping mode.

Synthesis of tetrahedron probe. DNA tetrahedron probes were synthesized through mixing the

four DNA strands (T_A, T_B, T_C, T_D) (Table S1) in stoichiometric equivalents in a buffer solution, followed by heated to 95℃ for 2 min and then rapidly cooled to 4℃. The tetrahedron platform consists of a pendant probe at one vertex to anchor the targets and three amino groups at the other three vertices to immobilize on the amine chip using cross-linker BS^3. At the same time, the characterizations of the synthetic product were executed by native polyacrylamide gel electrophoresis (PAGE) and atomic force microscopy (AFM).

Native polyacrylamide gel electrophoresis (PAGE). 12.5 μM DNAs were mixed with 6× loading buffer and then analyzed in 12% native polyacrylamide gel. Then the bands were stained by silver ions.[52] The photo of gel was taken by HUAWEI P9.

Preparation of amino sensor chip surface. The preparation of amino-modified sensor chip is carried out according to the reported method.[38,40] Unmodified silicon oxynitride AnaChip was firstly cleaned for 3 h with Piranha solution at 70℃. Subsequently, it was rinsed under sonication and then dried under a stream of nitrogen. The cleaned, dried, and unmodified sensor chip was silanized with 10% (v/v) APTES solution for 2 h at 30℃ in dark. After that, the sensor chip was fully rinsed three times with ethanol and ultrapure water respectively, finally blew dry under a steam of nitrogen.

DPI Experiments. The interaction of G-rich oligonucleotide sequence and Pb^{2+} on tetrahedron platform was real-time recorded employing a DPI instrument. The calibration process and construction of layer-by-layer assembly platform were same as our groups report,[38] merely substituting the probe. The process of building tetrahedron platform was as follows. Firstly, 250 μL BS^3 (2 mg/mL) was applied to both channels at 100 μL/min, then HEPES buffer returned to both channel and rinsed for 4 min. Secondly, 8 μM tetrahedron probes were steadily injected for 30 s at 100 μL/min, then 10 μL/min for 10 min. After injection, the flow was incubated for 5 min.

Thirdly, when the stable baseline was reached, Pb^{2+} with increased concentration was injected for 4 min, respectively. Finally, the experiment can be stopped until the steady baseline was obtained again.

RESULTS AND DISCUSSION

Native PAGE and AFM analysis of the tetrahedron probe. The 3D nanostructure consists of a pendant probe at one vertex to anchor the targets and three amino groups at the other three vertices to immobilize on the amine chip. The DNA tetrahedron was assembled from four DNA strands (T_A, T_B, T_C, T_D in Table S1) in stoichiometric equivalents by simply heating and "snap cooling". To verify the successful synthesis of tetrahedron probe, native PAGE (Figure S1) and AFM (Figure S2) were performed. As shown in Figure S1, the obvious bands in lane 1-4 indicated the shift position of one stand. And the shift distance of two combined stands were shown in lane 5-8, the higher bands displayed in lane 11-13 were the three combined stands. The highest bands in lane 9-10 demonstrated the formation of the tetrahedron. These control experiments displayed that the tetrahedron migrated more slowly than any other combinations of different stands, confirming the successful fabrication of the nanostructure. The tetrahedron shape and height (about 7 nm) shown by AFM image also demonstrated the successful construction of the tetrahedron probe.[53]

Characterization of interaction between G-rich nucleotide and Pb^{2+}. We utilized CD and UV-Vis differential spectrometry to investigate whether the designed probes could interact with Pb^{2+} or not. Figure 1A demonstrated that the CD spectra of tetrahedron probe exhibited two increased positive peaks at 220 nm and 265 nm when Pb^{2+} was added into the probe solution. Oppositely, the CD spectra of control probes showed negligible change after the addition of Pb^{2+}

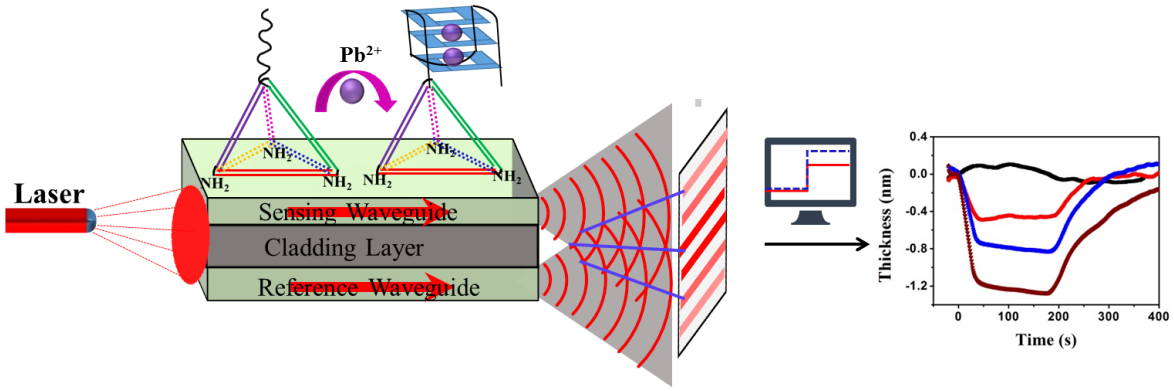

Scheme 1. Combination DNA tetrahedron with dual polarization interferometry technique for the study of interaction between G-rich DNA oligonucleotides and Pb^{2+}.

(shown in Figure 1B). The CD differential spectra were performed to clearly show the structural transition (Figure 1C). These results demonstrated that the designed probes could bind with Pb^{2+} and form parallel G-quadruplex structure.[54,55] To further verify the conversion is derived from the formation of G- quadruplex, the UV-Vis differential spectrometry was displayed in Figure 1D. The spectra of the target probe exhibited a negative peak around 295 nm, but the control probe showed negligible changes. The results were in line with previous report about hyperchroism at 295 nm originates in specific guanine–guanine stacking in the formation process of G-quadruplexes.[56]

Advantages of sensing probe immobilized on tetrahedron platforms. The immobilization process of tetrahedron platform was different from reported layer-by-layer assembly platform. Firstly, as shown in Figure 2, the immobilization time was significantly reduced. The layer-by-layer assembly sensing surface was successfully constructed by introducing polycation complex polyethylenimine (PEI) to link the unmodified chip and DNA probe. When the PEI was replaced by the running buffer in the channel, the sensing surface had evident structural changes due to the swelling property of PEI. Furthermore the stable baseline is difficult to obtain. While the

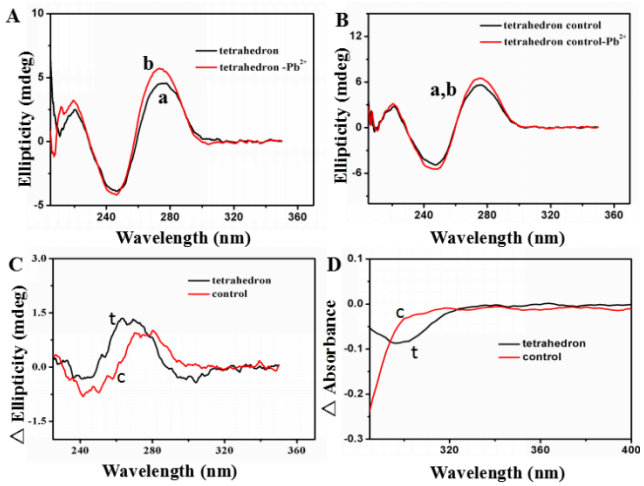

Figure 1. Characterization with Circular Dichroism and UV-vis spectrum. The CD spectrum of (A) tetrahedron, (B) tetrahedron control in the absence (a) and presence (b) of Pb^{2+}. The CD (C) and UV-Vis (D) differential spectrometry between tetrahedron (t) and tetrahedron control (c).

fabrication of tetrahedron sensing platform (Scheme 1) was implemented by immobilizing NH_2-tetrahedron probe to amine-modified chip using BS^3 linker.[57] Once the surface is activated, the tetrahedron probe should be immobilized as quickly as possible because the NHS ester of the BS^3 would hydrolyze whilst exposed to the running buffer. Secondly, Table 1 showed the standard deviation of key parameters on tetrahedron platform is smaller than that on the layer-by-layer platform, reflecting the higher reproducibility of tetrahedron platform. Simultaneously, the major parameters revealed that loading mass per area on layer-by-layer assembly platform (0.8 ng/mm^2) was two times higher than that on tetrahedron platform (0.4 ng/mm^2), while it had less change in thickness (2 nm on layer-by-layer assembly platform, 3.5 nm on tetrahedron platform). Furthermore, the density decreased by about 10% on the layer-by-layer assembly platform after introducing probes. In contrast, 50% decrease was obtained on the tetrahedron platform. Based on these phenomena, we speculated that the probes on the layer-by-layer assembly platform might stabilize in a tilting conformation, while the probes stand upright on the tetrahedron

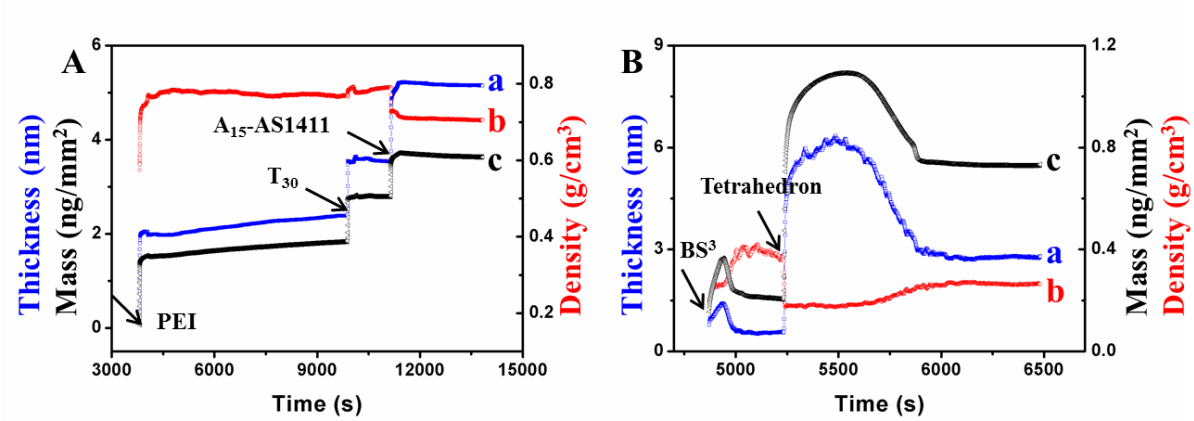

Figure 2. Construction processes of two different sensing platforms. Real-time thickness (a), density (b), mass (c) in the immobilization process of layer-by-layer assembly (A) and tetrahedron (B) platforms.

platform (Scheme 1) at defined nanoscale distances. Thirdly, in order to explicitly understand the dynamic process of tetrahedron probe, we plotted the thickness and density changes as a function of the mass, respectively.[59,60] As displayed in Figure 3, the thickness and density changes were plotted a closed loop as the mass changes, demonstrating the tetrahedron platform was regenerable (The corresponding details were discussed in the following section).

Interaction of G-rich ssDNA-Pb^{2+}. Based on above advantages of tetrahedron, the highly ordered tetrahedron platform was developed to study the interaction of G-rich ssDNA and Pb^{2+} using DPI. From the above data, we could roughly speculate the whole interaction process of G-rich ssDNA-Pb^{2+}. Initially, the probes stood on the chip in a loose and thick state because the DNA tetrahedrons were immobilized at defined nanoscale distances on the interface. After adding Pb^{2+} into the channel, the mass and density increased, but the thickness decreased, indicating a thinner but denser layer was formed because the converging G-quadruplex filled the vacation. It is believed that the random coil structure of G-rich ssDNA was converted into G-quadruplex because Pb^{2+} has higher structural stability for G-rich ssDNA.[58] Besides, based on

the changes rules of thickness and density as the mass (see Figure 3), we could not only quantify the extent of probes structural changes, but also obtain assisted dynamic structural information for the whole interaction process. From the trend of structural changes in Figure 3A-B, the thickness increased and the density decreased with the increasing of mass at low Pb^{2+} concentration. One possible reason might be that the low Pb^{2+} concentration is not enough to quickly form folded G-quadruplex, but enabled the random coil ssDNA probes to have a stretch because the increased ions strength could minimize repulsion between DNA chains.[40] At high Pb^{2+} concentration as shown in Figure 3C-D, the thickness decreased and the density increased with the increasing of mass. Here, we had demonstrated a complete interaction process in detail by combining Scheme 2, taking the process at low Pb^{2+} concentration as an example. From the intensive degree of data points, we could obtain the adsorption rate because the data collected at the same time interval. As we can see, the whole process was split three steps by a turning region (S). Before the S region, the data points were scattered, suggesting the adsorption rate was fast. The results also reflected the process that G- rich ssDNA formed primary G-quartets by H-bonding and cation binding, which corresponded to the Step 1 of Scheme 2. In the S region, the points were dense, suggesting the association and disassociation gradually reached equilibrium.

Table 1. Key Parameters of Different Layers in the Two Platforms.

	Layers	RI	Thickness(nm)	Mass(ng/mm^2)	Density(g/cm^3)
Tetrahedron Platform	BS^3	1.359±0.001	2.053±0.158	0.285±0.040	0.139±0.072
	Tetrahedron/BS^3	1.347±0.005	5.556±0.264	0.652±0.075	0.069±0.027
Layer-by-Layer Assembly Platform	PEI	1.457±0.012	2.140± 0.357	1.476±0.221	0.693±0.065
	T_{30}/PEI	1.460±0.013	3.786±0.704	2.671 ±0.422	0.711±0.076
	Probe/T_{30}/PEI	1.443±0.016	5.783± 1.154	3.485±0.568	0.611±0.094

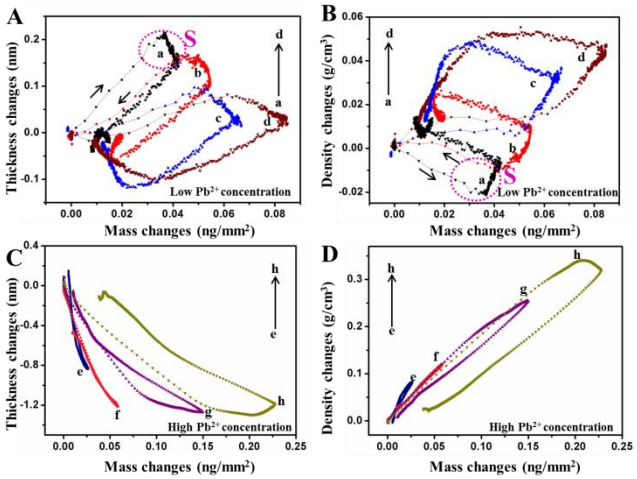

Figure 3. The whole dynamic formation process of G-quadruplex at different Pb^{2+} concentration. The change rules of layer thickness (A, C) and density (B, D) as respective mass were studied under low (A, B) and high (C, D) Pb^{2+} concentration. The Pb^{2+} concentrations from a to h: 2, 4, 6, 8, 200, 400, 600, 800 μM. The short arrows show the start and end of interaction process. The magenta loop S shows the turning region.

This phenomenon showed that intermediates of G-rich ssDNA folded into compact and stable G-quadruplex topologies by relatively slow strand rearrangements, which corresponded to the Step 2 of Scheme 2. Behind the S region, the thickness and density returned to the original position at a slower rate, inferring that the G-quadruplexes were nearly dissociated, which corresponded to the Step 3 of Scheme 2. The study gave an evidence for the fact that G-quadruplex did not form rapidly, while underwent a structural adjustment as shown in Scheme 2. The result is consistent with other reports about the dynamic forming process of G- quadruplex.[24,26,61]

Establishment of Pb^{2+} biosensor. As depicted in Figure 4A-D, with the increase of the Pb^{2+} concentration, the mass and density increased, and the thickness decreased fast until achieving balance. When the running buffer flowed past the channel, the mass, thickness, and the density almost returned to the original position, demonstrating that the Pb^{2+}-stabilized G-quadruplex

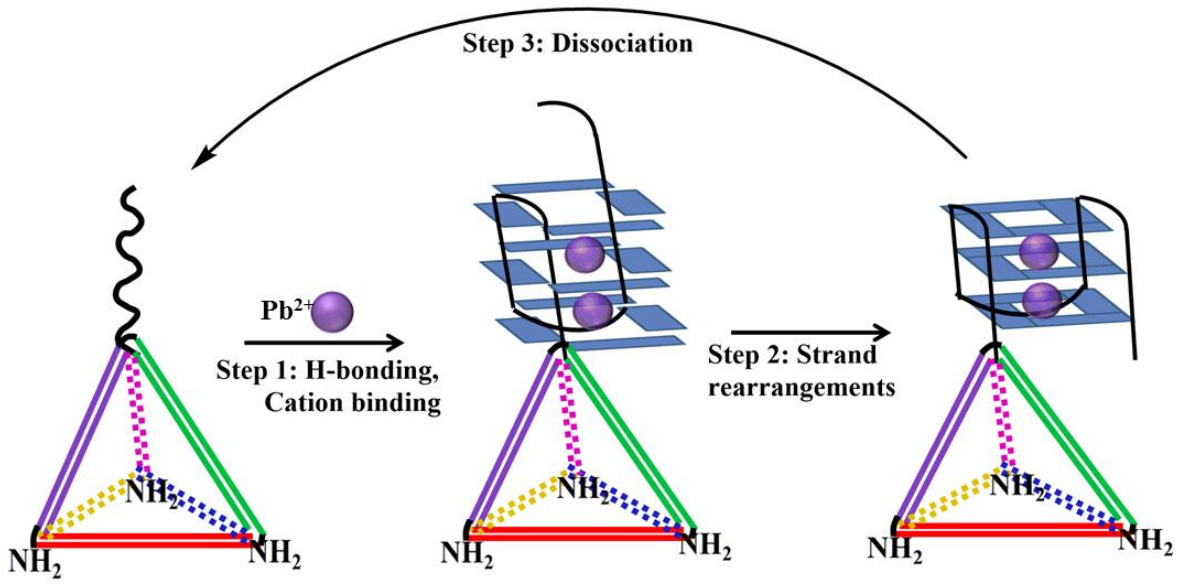

Scheme 2. The schematic diagram for the formation and dissociation process of G-quadruplex.

complex on tetrahedron platform was allowed to fully dissociate. Moreover, the mass, density, RI and thickness changes were proportional to the Pb^{2+} concentration from 1 μM to 800 μM. When the concentration exceeded 600 μM, the structural parameters changed in different trends. It may attribute to the different binding way and the already saturated binding sites. Based on the preceding results, a biosensor for the detection of Pb^{2+} was fabricated on the tetrahedron probe platform. As the concentration increasing from 1 μM to 20 μM, the mass, density, RI and thickness (Figure 4E-H) were linearly related with the Pb^{2+} concentration. In term of different calibration methods, such as mass, thickness, density and RI, several detection limits were obtained (9 nM, 1.83 nM, 14.2 nM, 11.5 nM, respectively), and much lower than the lead limit of 0.24 μM in drinking water established by World Health Organization (WHO), as well as comparable to previously reported methods for Pb^{2+} detection (Table S2).

Specificity and Selectivity of Pb^{2+} biosensor. To justify the specificity of the biosensor, the complementary probe acted as the substitute to investigate the binding condition. As displayed in

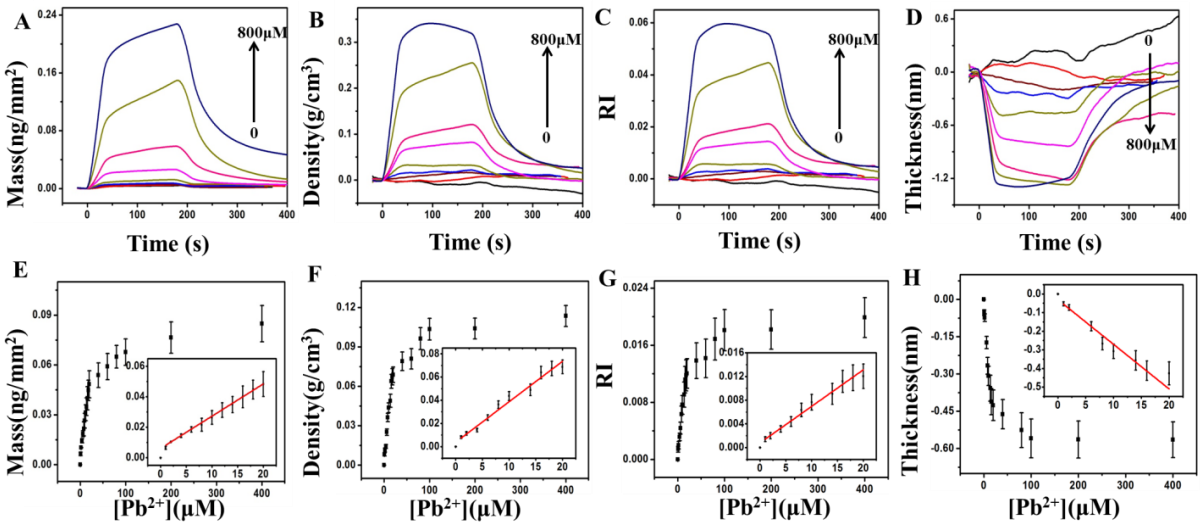

Figure 4. Structural changes trends and linearity of Pb^{2+} biosensor. Real-time mass, density, RI, and thickness changes of the tetrahedron probe (A-D) upon Pb^{2+} injection. The arrows show increasing Pb^{2+} concentration. The lines were smoothed by software OriginPro 8.0. Plots of mass, density, RI, thickness changes (E-H) of Pb^{2+} concentration ranging from 1 μM to 400 μM. Inset: expanded linear region.

Figure S3, the thickness, RI, mass, and density changes for target probe were much more distinct than the control probe when Pb^{2+} with different concentrations were added, inferring Pb^{2+} specifically bound with G-rich ssDNA. In addition, the selectivity experiments were implemented by comparing with control metal ions such as Cs^{+}, Ca^{2+}, Na^{+}, Mg^{2+}, Zn^{2+}, Mn^{2+}, and K^{+}. As demonstrated in Figure 5, the mass, density, and thickness changes caused by introduction of these ions were unconspicuous when compared with Pb^{2+}, showing the high selectivity of this Pb^{2+} biosensor on the 3D platform.

Detection of EDTA. EDTA, as a representative material of the important complexing agents, can be widely applied as dyeing auxiliaries, blood anticoagulant, and detergent. However, its negative impacts including irritating the skin and mucous membrane, causing the asthma, skin

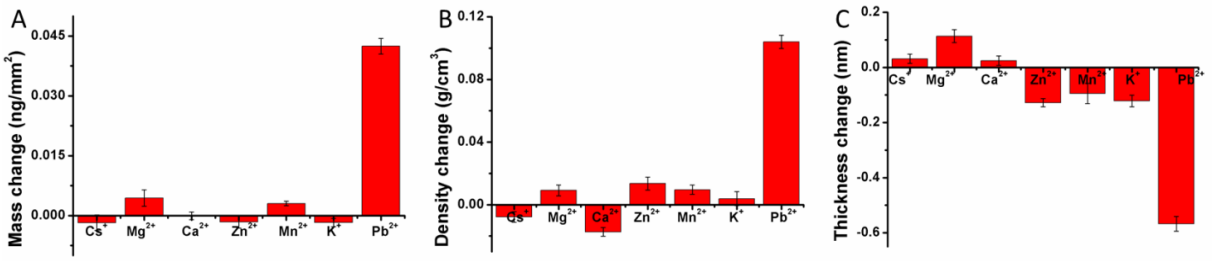

Figure 5. Selectivity of Pb^{2+} biosensor. Histograms of mass (A), density (B), thickness (C) changes. The concentration of interfering ions such as Cs^{+}, Ca^{2+}, Mg^{2+}, Zn^{2+}, Mn^{2+}, K^{+} and Pb^{2+} was 100 μM.

rashes become increasingly prominent. Therefore, it is essential to develop high sensitive method for the determination of EDTA. According to the strong chelation between Pb^{2+} and EDTA, the Pb^{2+}-stabilized G-quadruplex can be used to detect EDTA. In the presence of EDTA, the conformational transition of the probe from single strand to G-quadruplex was hindered. Hence, the mass and density decreased as the increase of EDTA concentration, while the thickness showed contrary trend as shown in Figure S4A-C. The changes exhibited a linear relationship to the EDTA concentration. In addition, EDTA obviously suppressed the structural transition, while the control chelates had no evident interference on the structural changes (in Figure S4D-F). These results inferred that a sensitive and specific EDTA biosensor with low detection limits (15 nM for mass, 2 nM for thickness, and 28 nM for density) was successfully fabricated.

Application of the DNA tetrahedron platform in real samples. To validate the practical value of the DNA tetrahedron-assisted biosening platform, the detection of Pb^{2+} in lake water was carried out. We spiked Pb^{2+} of different concentrations into the 1% real sample diluted with running buffer and detect the real concentration using DPI technique. As shown in Table S3, four groups of concentration data were obtained based on RI, mass, thickness, and density calibrations. The recoveries ranged from 93.95% to 101.5% with the RSDs from 3.51% to 12.8%.

Additionally, the results detected with the present method were consistent with those of the ICP-AES method, suggesting the potential of this developed analytical method in the determination of real samples.

CONCLUSION

In conclusion, a stable, ordered, predictable, and easily prepared DNA tetrahedron nanostructure was combined with DPI to investigate the interaction between G-rich nucleotide and Pb^{2+}. This method overcame probe accessibility problem existed in surface technique, which not only more veraciously reflected the behavior of probe-target interaction, but also improved the sensitivity of biosensor. Compared to the layer-by-layer assembly platform, the tetrahedron platform has higher reproducibility, regenerative ability and time-efficient immobilization process. Therefore, it is the icing on the cake of biosensor to introduce surface chemistry. In addition, the detailed structural dynamics for the interaction process of G-quadruplex with Pb^{2+} laid a foundation for the exploring the interaction of G-quadruplex with other targets, e.g. drugs and pathogenes. Therefore, the developed method paves the road to intensely research the G-quadruplex-related neurodegenerative disease and other receptor-ligand interaction by changing the probes and the corresponding targets.

ASSOCIATED CONTENT

Supporting Information. The Supporting Information is available free of charge on the ACS Publications website. Table S1, all the sequences used in experiment; Figure S1-2, native PAGE and AFM characterization of tetrahedron probe, Figure S3, comparison testing for target and control strands; Figure S4, linear changes and selectivity of EDTA biosensor.

AUTHOR INFORMATION

Corresponding Author

*Prof. Xiurong Yang, State Key Laboratory of Electroanalytical Chemistry, Changchun Institute of Applied Chemistry, Chinese Academy of Sciences. E-mail: xryang@ciac.ac.cn Tel.: +86 431 85262056; Fax: +86 431 85689278.

Author Contributions

The experiments and manuscript were mainly accomplished by Shuang Wang under help and guidance of Prof. Xiurong Yang and Dr. Jianshe Huang. All authors have a contribution to the revision of final manuscript.

Notes

The authors declare no competing financial interest.

ACKNOWLEDGMENT

This work was financially supported by the National Natural Science Foundation of China (No. 21435005, 21627808) and Key Research Program of Frontier Sciences, CAS (QYZDY-SSW-SLH019)

REFERENCES

(1) Han, H.; Hurley, L. H. G-quadruplex DNA: A Potential Target for Anti-cancer Drug Design. *Trends. Pharmacol. Sci.* **2000**, *21* (4), 136-142.

(2) You, H.; Zeng, X.; Xu, Y.; Lim, C. J.; Efremov, A. K.; Phan, A. T.; Yan, J. Dynamics and Stability of Polymorphic Human Telomeric G-quadruplex under Tension. *Nucleic. Acids. Res.* **2014**, *42* (13), 8789-8795.

(3) Nakken, S.; Rognes, T.; Hovig, E. The Disruptive Positions in Human G-quadruplex Motifs

are Less Polymorphic and More Conserved than Their Neutral Counterparts. *Nucleic. Acids. Res.* **2009**, *37* (17), 5749-5756.

(4) Eddy, J.; Maizels, N. Conserved Elements with Potential to Form Polymorphic G-quadruplex Structures in the First Intron of Human Genes. *Nucleic. Acids. Res.* **2008**, *36* (4), 1321-1333.

(5) Lemmens, B.; Van Schendel, R.; Tijsterman, M. Mutagenic Consequences of a Single G-quadruplex Demonstrate Mitotic Inheritance of DNA Replication Fork Barriers. *Nat. Commun.* **2015**, *6*, 8909.

(6) Grigg, J. C.; Shumayrikh, N.; Sen, D. G-Quadruplex Structures Formed by Expanded Hexanucleotide Repeat RNA and DNA from the Neurodegenerative Disease-Linked C9orf72 Gene Efficiently Sequester and Activate Heme. *Plos. One.* **2014**, *9* (9), e106449.

(7) Taylor, J. P. Neurodegenerative Diseases: G-quadruplex Poses Quadruple Threat. *Nature* **2013**, *507* (7491), 175-177.

(8) Simone, R.; Fratta, P.; Neidle, S.; Parkinson, G. N.; Isaacs, A. M. G-quadruplexes: Emerging Roles in Neurodegenerative Diseases and the Non-coding Transcriptome. *FEBS Lett.* **2015**, *589* (14), 1653-1668.

(9) Ivanov, P.; O'Day, E.; Emara, M. M.; Wagner, G.; Lieberman, J.; Anderson, P. G-quadruplex Structures Contribute to the Neuroprotective Effects of Angiogenin-induced tRNA Fragments. *Proc. Natl Acad. Sci. U. S. A.* **2014**, *111* (51), 18201-18206.

(10) De Feijter, J. A.; Benjamins, J.; Veer, F. A. Ellipsometry as a Tool to Study the Adsorption Behavior of Synthetic and Biopolymers at the Air–water Interface. *Biopolymers* **1978**, *17* (7), 1759-1772.

(11) Kypr, J.; Kejnovská, I.; Renčiuk, D.; Vorlíčková, M. Circular Dichroism and Conformational Polymorphism of DNA. *Nucleic. Acids. Res.* **2009**, *37* (6), 1713-1725.

(12) Mergny, J.-L.; Phan, A.-T.; Lacroix, L. Following G-quartet Formation by UV-spectroscopy. *FEBS Lett.* **1998**, *435* (1), 74-78.

(13) Rachwal, P. A.; Fox, K. R. Quadruplex Melting. *Methods* **2007**, *43* (4), 291-301.

(14) De Cian, A.; Guittat, L.; Kaiser, M.; Saccà, B.; Amrane, S.; Bourdoncle, A.; Alberti, P.; Teulade-Fichou, M.-P.; Lacroix, L.; Mergny, J.-L. Fluorescence-based Melting Assays for Studying Quadruplex Ligands. *Methods* **2007**, *42* (2), 183-195.

(15) Okamoto, K.; Sannohe, Y.; Mashimo, T.; Sugiyama, H.; Terazima, M. G-quadruplex Structures of Human Telomere DNA Examined by Single Molecule FRET and BrG-substitution. *Bioorgan. Med. Chem.* **2008**, *16* (14), 6873-6879.

(16) Ying, L.; Green, J. J.; Li, H.; Klenerman, D.; Balasubramanian, S. Studies on the Structure and Dynamics of the Human Telomeric G quadruplex by Single-molecule Fluorescence Resonance Energy Transfer. *Proc. Natl. Acad. Sci. U. S. A.* **2003**, *100* (25), 14629-14634.

(17) Kumar, N.; Maiti, S. A Thermodynamic Overview of Naturally Occurring Intramolecular DNA Quadruplexes. *Nucleic. Acids. Res.* **2008**, *36* (17), 5610-5622.

(18) Petraccone, L.; Spink, C.; Trent, J. O.; Garbett, N. C.; Mekmaysy, C. S.; Giancola, C.; Chaires, J. B. Structure and Stability of Higher-Order Human Telomeric Quadruplexes. *J. Am. Chem. Soc.* **2011**, *133* (51), 20951-20961.

(19) Majhi, P. R.; Qi, J.; Tang, C.-F.; Shafer, R. H. Heat Capacity Changes Associated with Guanine Quadruplex Formation: An Isothermal Titration Calorimetry Study. *Biopolymers* **2008**, *89* (4), 302-309.

(20) Fan, H. Y.; Shek, Y. L.; Amiri, A.; Dubins, D. N.; Heerklotz, H.; Macgregor, R. B.; Chalikian, T. V. Volumetric Characterization of Sodium-Induced G-Quadruplex Formation. *J. Am. Chem. Soc.* **2011**, *133* (12), 4518-4526.

(21) Sannohe, Y.; Endo, M.; Katsuda, Y.; Hidaka, K.; Sugiyama, H. Visualization of Dynamic Conformational Switching of the G-Quadruplex in a DNA Nanostructure. *J. Am. Chem. Soc.* **2010**, *132* (46), 16311-16313.

(22) Zhang, A. Y. Q.; Balasubramanian, S. The Kinetics and Folding Pathways of Intramolecular G-Quadruplex Nucleic Acids. *J. Am. Chem. Soc.* **2012**, *134* (46), 19297-19308.

(23) Gray, R. D.; Chaires, J. B. Kinetics and Mechanism of K^+- and Na^+-induced Folding of Models of Human Telomeric DNA into G-quadruplex Structures. *Nucleic. Acids. Res.* **2008**, *36* (12), 4191-4203.

(24) Mashimo, T.; Yagi, H.; Sannohe, Y.; Rajendran, A.; Sugiyama, H. Folding Pathways of Human Telomeric Type-1 and Type-2 G-quadruplex Structures. *J. Am. Chem. Soc.* **2010**, *132* (42), 14910-14918.

(25) You, H.; Zeng, X.; Xu, Y.; Lim, C. J.; Efremov, A. K.; Phan, A. T.; Yan, J. Dynamics and Stability of Polymorphic Human Telomeric G-quadruplex under Tension. *Nucleic. Acids. Res.* **2014**, *42* (13), 8789-8795.

(26) Li, W.; Hou, X.-M.; Wang, P.-Y.; Xi, X.-G.; Li, M. Direct Measurement of Sequential Folding Pathway and Energy Landscape of Human Telomeric G-quadruplex Structures. *J. Am. Chem. Soc.* **2013**, *135* (17), 6423-6426.

(27) Huber, W.; Barner, R.; Fattinger, C.; Hübscher, J.; Koller, H.; Müller, F.; Schalatter, D.; Lukosz, W. Direct Optical Immunosensing (Sensitivity and Selectivity). *Sensor. Actuat B: Chem.***1992**, *6* (1), 122-126.

(28) Schneider, B. H.; Edwards, J. G.; Hartman, N. F. Hartman Interferometer: Versatile Integrated Optic Sensor for Label-free, Real-time Quantification of Nucleic Acids, Proteins, and Pathogens. *Clin. Chem.* **1997**, *43* (9), 1757-1763.

(29) Freeman, N. Dual Polarisation Interferometry: An Optical Technique to Measure the Orientation and Structure of Proteins at the Solid-Liquid Interface in Real Time. *Proteins. Solid-Liquid. Interfaces*, Déjardin, P., Ed. Springer Berlin Heidelberg: Berlin, Heidelberg, **2006**, 75-104.

(30) Song, H.; Sun, W.; Prabhakar, S.; Aung, K. M. M.; Su, X. Study Sequence Rules of Estrogen Receptor α–DNA Interactions Using Dual Polarization Interferometry and Computational Modeling. *Anal. Biochem.* **2013**, *433* (2), 121-128.

(31) Yao, D.; Song, T.; Sun, X.; Xiao, S.; Huang, F.; Liang, H. Integrating DNA-Strand-Displacement Circuitry with Self-Assembly of Spherical Nucleic Acids. *J. Am. Chem. Soc.* **2015**, *137* (44), 14107-14113.

(32) Wan, Y.; Li, X. Two-dimensional Nuclear Magnetic Resonance Spectroscopy with Parallel Acquisition of 1H-1H and 19F-19F Correlations. *Chinese. J. Anal. Chem.* **2015**, *43* (8), 1203-1209.

(33) Huang, G.; Yuan, L.; Liu, S.; Zhou, S. In Situ Phosphitylation for Nuclear Magnetic Resonance Identification of Precursors of Chemical Warfare Agents. *Chinese. J. Anal. Chem.* **2015**, *43* (12), 1927-1933.

(34) Escorihuela, J.; Gonzalez-Martinez, M. A.; Lopez-Paz, J. L.; Puchades, R.; Maquieira, A.; Gimenez-Romero, D. Dual Polarization Interferometry: A Novel Technique to Light up the Nanomolecular World. *Chem. Rev.* **2015**, *115* (1), 265-294.

(35) Levicky, R.; Herne, T. M.; Tarlov, M. J.; Satija, S. K. Using Self-Assembly to Control the Structure of DNA Monolayers on Gold: A Neutron Reflectivity Study. *J. Am. Chem. Soc.* **1998**, *120* (38), 9787-9792.

(36) Irving, D.; Gong, P.; Levicky, R. DNA Surface Hybridization: Comparison of Theory and

Experiment. *J. Phys. Chem. B.* **2010**, *114* (22), 7631-7640.

(37) Zheng, Y.; Hu, T.; Chen, C.; Yang, F.; Yang, X. An Anti-fouling Aptasensor for Detection of Thrombin by Dual Polarization Interferometry. *Chem. Commun.* **2015**, *51* (26), 5645-5648.

(38) Zheng, Y.; Yang, C.; Yang, F.; Yang, X. Real-Time Study of Interactions between Cytosine−Cytosine Pairs in DNA Oligonucleotides and Silver Ions Using Dual Polarization Interferometry. *Anal. Chem.* **2014**, *86* (8), 3849-3855.

(39) Wang, Y.; Zheng, Y.; Yang, F.; Yang, X. Dual Polarisation Interferometry for Real-time, Label-free Detection of Interaction of Mercury(II) with Mercury-specific Oligonucleotides. *Chem. Commun.* **2012**, *48* (23), 2873-2875.

(40) Huang, F.; Xu, P.; Liang, H. Using Dual Polarization Interferometry to Study Surface-initiated DNA Hybridization Chain Reactions in Real time. *Biosens. Bioelectron.* **2014**, *51*, 317-323.

(41) Yan, H. Nucleic Acid Nanotechnology. *Science* **2004**, *306* (5704), 2048-2049.

(42) Lin, C.; Katilius, E.; Liu, Y.; Zhang, J.; Yan, H. Self-Assembled Signaling Aptamer DNA Arrays for Protein Detection. *Angew. Chem.* **2006**, *118* (32), 5422-5427.

(43) Zhang, Z.; Wang, Y.; Fan, C.; Li, C.; Li, Y.; Qian, L.; Fu, Y.; Shi, Y.; Hu, J.; He, L. Asymmetric DNA Origami for Spatially Addressable and Index-Free Solution-Phase DNA Chips. *Adv. Mater.* **2010**, *22* (24), 2672-2675.

(44) Winfree, E.; Liu, F.; Wenzler, L. A.; Seeman, N. C. Design and Self-assembly of Two-dimensional DNA Crystals. *Nature* **1998**, *394* (6693), 539-544.

(45) Wang, S.; Zhang, L.; Wan, S.; Cansiz, S.; Cui, C.; Liu, Y.; Cai, R.; Hong, C.; Teng, I. T.; Shi, M.; Wu, Y.; Dong, Y.; Tan, W. Aptasensor with Expanded Nucleotide Using DNA Nanotetrahedra for Electrochemical Detection of Cancerous Exosomes. *ACS Nano* **2017**, *11* (4),

3943-3949.

(46) Xie, N.; Huang, J.; Yang, X.; Yang, Y.; Quan, K.; Wang, H.; Ying, L.; Ou, M.; Wang, K. A DNA Tetrahedron-based Molecular Beacon for Tumor-related mRNA Detection in Living Cells. *Chem. Commun.* **2016**, *52* (11), 2346-2349.

(47) Chen, X.; Zhou, G.; Song, P.; Wang, J.; Gao, J.; Lu, J.; Fan, C.; Zuo, X. Ultrasensitive Electrochemical Detection of Prostate-Specific Antigen by Using Antibodies Anchored on a DNA Nanostructural Scaffold. *Anal. Chem.* **2014**, *86* (15), 7337-7342.

(48) Zhou, G.; Lin, M.; Song, P.; Chen, X.; Chao, J.; Wang, L.; Huang, Q.; Huang, W.; Fan, C.; Zuo, X. Multivalent Capture and Detection of Cancer Cells with DNA Nanostructured Biosensors and Multibranched Hybridization Chain Reaction Amplification. *Anal. Chem.* **2014**, *86* (15), 7843-7848.

(49) Li, J.; Fan, C.; Pei, H.; Shi, J.; Huang, Q. Smart Drug Delivery Nanocarriers with Self-Assembled DNA Nanostructures. *Adv. Mater.* **2013**, *25* (32), 4386-4396.

(50) Wen, Y.; Pei, H.; Wan, Y.; Su, Y.; Huang, Q.; Song, S.; Fan, C. DNA Nanostructure-Decorated Surfaces for Enhanced Aptamer-Target Binding and Electrochemical Cocaine Sensors. *Anal. Chem.* **2011**, *83* (19), 7418-7423.

(51) Pei, H.; Lu, N.; Wen, Y.; Song, S.; Liu, Y.; Yan, H.; Fan, C. A DNA Nanostructure-based Biomolecular Probe Carrier Platform for Electrochemical Biosensing. *Adv. Mater.* **2010**, *22* (42), 4754-4758.

(52) Shevchenko, A.; Wilm, M.; Vorm, O.; Mann, M. Mass Spectrometric Sequencing of Proteins from Silver-Stained Polyacrylamide Gels. *Anal. Chem.* **1996**, *68* (5), 850-858.

(53) Pei, H.; Wan, Y.; Li, J.; Hu, H.; Su, Y.; Huang, Q.; Fan, C. Regenerable Electrochemical Immunological Sensing at DNA Nanostructure-decorated Gold Surfaces. *Chem. Commun.* **2011**,

47 (22), 6254-6256.

(54) Knoller, S.; Shpungin, S.; Pick, E. The Membrane-associated Component of the Amphiphile-activated, Cytosol-dependent Superoxide-forming NADPH Oxidase of Macrophages is Identical to Cytochrome b559. *J. Biol. Chem.* **1991**, *266* (5), 2795-2804.

(55) Kypr, J.; Kejnovska, I.; Renciuk, D.; Vorlickova, M. Circular Dichroism and Conformational Polymorphism of DNA. *Nucleic. Acids. Res.* **2009**, *37* (6), 1713-1725.

(56) Karsisiotis, A. I.; Hessari, N. M. a.; Novellino, E.; Spada, G. P.; Randazzo, A.; Webba da Silva, M. Topological Characterization of Nucleic Acid G-Quadruplexes by UV Absorption and Circular Dichroism. *Angew. Chem. Int. Ed.* **2011**, *50* (45), 10645-10648.

(57) Mergny, J. L.; Li, J.; Lacroix, L.; Amrane, S.; Chaires, J. B. Thermal Difference Spectra: A Specific Signature for Nucleic Acid Structures. *Nucleic. Acids. Res.* **2005**, *33* (1), 81-94.

(58) Li, T.; Wang, E.; Dong, S. Potassium−Lead-Switched G-Quadruplexes: A New Class of DNA Logic Gates. *J. Am. Chem. Soc.* **2009**, *131* (42), 15082-15083.

(59) Wang, J.; Xu, X.; Zhang, Z.; Yang, F.; Yang, X. Real-Time Study of Genomic DNA Structural Changes upon Interaction with Small Molecules Using Dual-Polarization Interferometry. *Anal. Chem.* **2009**, *81* (12), 4914–4921.

(60) Wang, Y.; Wang, J.; Yang, F.; Yang, X. Probing Biomolecular Interactions with Dual Polarization Interferometry: Real-time and Label-free Coralyne Detection by Use of Homoadenine DNA Oligonucleotide. *Anal. Chem.* **2012**, *84* (2), 924-930.

(61) Chaires, J. B. Human Telomeric G-quadruplex: Thermodynamic and Kinetic Studies of Telomeric Quadruplex Stability. *FEBS J.* **2010**, *277* (5), 1098-1106.

Table of Contents Graphic and Synopsis

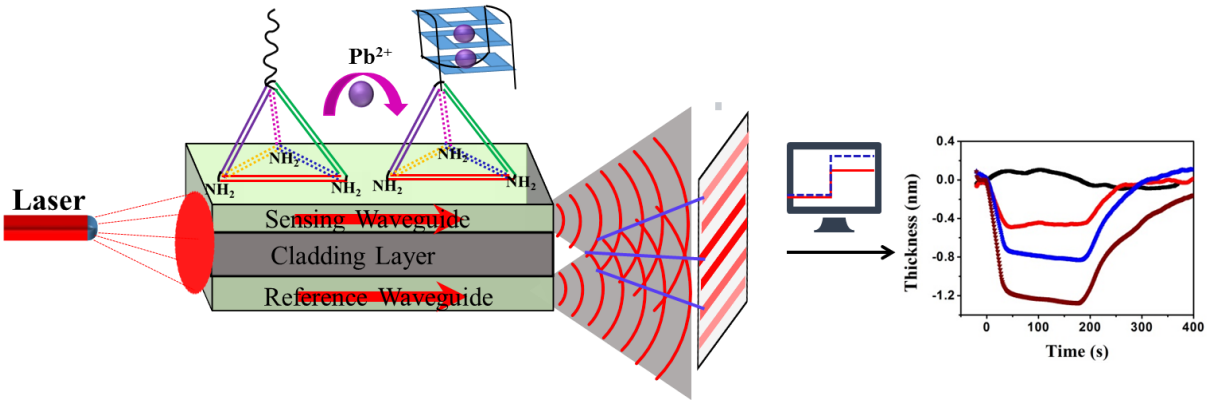

Combination DNA tetrahedron with DPI technique for the study of interaction between G-rich DNA oligonucleotides and Pb^{2+}.